Case Studies in Thermal Engineering 62 (2024) 105186

Contents lists available at ScienceDirect

Case Studies in Thermal Engineering

journal homepage: www.elsevier.com/locate/csite

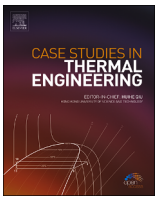

Numerical simulation of the impact of rainfall on tunnel fire

Dia Luan [a, b], Jakub Bielawski [b, c], Chuangang Fan [a, *], Wojciech Węgrzyński [c], Xinyan Huang [b, **]

[a] School of Civil Engineering, Central South University, Changsha, China
[b] Department of Building Environment and Energy Engineering, The Hong Kong Polytechnic University, China
[c] Fire Research Department, Building Research Institute, 1 Filtrowa St., 00-611, Warsaw, Poland

HIGHLIGHTS

- Multi-hazards of tunnel fire and heavy rainfall considered.
- Model to investigate the interaction of tunnel fires and rainfall established.
- Fluid flow inside the tunnel under the impact of rainfall revealed.
- Thermocouple model effectively reduce predicted temperature verified.
- Real-scale fire hazards in tunnels under rainfall effect evaluated.

ARTICLE INFO

Keywords:
Multi-hazard
Tunnel fire
Rainfall effect
Extreme weather
Scale effect

ABSTRACT

An improved understanding of tunnel fire dynamics is crucial for fire and life safety. This work highlights the significance of Computational Fluid Dynamics (CFD) techniques in addressing the interaction between tunnel fires and rainfall. The discrete phase model based on the Lagrangian approach is applied to simulate raindrops, while the species transport model is used to simulate fuel combustion. A numerical model is established to investigate the impact of rainfall on tunnel fires, and the correctness of the model is verified by comparing the results to model-scale tunnel experiments. Results show that the raindrops increase the local pressure in the rainfall area, creating a pressure difference between the rainfall tunnel portal and the no-rain portal, which leads to longitudinal airflow inside the tunnel. This rain-induced airflow prevents smoke from moving toward the rainfall tunnel portal and decreases the smoke height near the no-rainfall portal. Correlations between the local increased pressure, induced-airflow velocity, and rainfall parameters are proposed. Besides, the model is scaled up to full-size, and real-scale tunnel fires under the influence of rainfall are evaluated. Findings draw attention to tunnel fire dynamics under extreme weather conditions for improved fire safety and evacuation strategies.

1. Introduction

With the intensification of climate change, extreme weather events, notably heavy rainfall, have become increasingly prevalent and severe. A notable example occurred in 2023 in Shenzhen City, Guangdong Province, China, where 57 days of intense local rainfall were recorded [1], underscoring the urgency of addressing the challenges posed by such events. Meanwhile, tunnels, as a crucial component of urban infrastructure, are facing a rise in fire accidents due to the growing number and complexity of structures. The com-

* Corresponding author.
** Corresponding author.
E-mail addresses: chuangang.fan@csu.edu.cn (C. Fan), xy.huang@polyu.edu.hk (X. Huang).

https://doi.org/10.1016/j.csite.2024.105186
Received 19 July 2024; Received in revised form 8 September 2024; Accepted 21 September 2024
Available online 22 September 2024

bined occurrence of rainfall and fire in tunnels poses a significant challenge, as the dynamics of these hazards can interact in complex ways. Despite the significant progress made in understanding the impact of rainfall on tunnel fire dynamics through our previous model-scale experiments [2–4], which have emphasized the crucial role of rainfall in altering fire behavior and smoke movement patterns, conducting full-scale fire tests in tunnels remains challenging. This study aims to bridge this gap by developing and validating a CFD (Computational Fluid Dynamics) model that captures the dynamics of real-size tunnel fires in the presence of heavy rainfall.

CFD tools have emerged as invaluable means for exploring the effects of extreme weather conditions in urban areas, including the influence of wind and rainfall on building facades, bridges, and transportation systems. For example, Węgrzyński et al. [5–8] investigated the influence of wind on the performance of natural smoke and heat exhaust systems for various ventilators using CFD simulations. They also provided some suggestions for coupled modeling of wind and fire. Kataoka et al. [9] summarized the applications and prospects of CFD tools in wind engineering, emphasizing its use in predicting pedestrian wind environments, dust dispersion, and wind forces on complex structures. Shirzadi et al. [10] provided some guidance and suggestions on using CFD models for wind field simulation in highly-packed urban areas. Blacken and Carmeliet [11] used ANSYS® Fluent to assess the spatial and temporal distribution of wind-driven rain (WDR) on the facade of a low-rise building. Kubilay et al. [12] investigated the influence of building configurations on the catch ratio of the WDR on two parallel wide buildings through simulation, and the results were validated with data from the field measurements. Gao et al. [13] investigated the impact of wind drift on the rainfall-runoff relationship in urban high-rise building areas, focusing on the relationship between wind speed and rainfall inclination through CFD method. Wang et al. [14–16] systematically examined the influences of wind speed, wind direction, and rainfall intensity on the WDR flow and distribution characteristics for building facades. Liu et al. [17] considered the turbulent dispersion of raindrops and evaluated the effects of WDR on bridges, including WDR flow fields, catch ratio, rain loads, and so on. Llarena et al. [18] assessed the rain mitigation performance under various roof alternatives for San Mames Stadium. Yu et al. [19] evaluated the aerodynamic characteristics of a high-speed train in heavy rain environments. Ouyang et al. [20] investigated the flow field around high-speed trains encountering the tunnel entrance under strong wind-rain environments and found that the amplification effect of rain on wind-rain loads may endanger the driving safety of trains at the tunnel entrance. Besides, the soil water dynamics and soil slope failure under rainfall conditions also investigated with CFD tools [21–23].

Furthermore, CFD tools are also widely used to study fire behaviors and smoke motions in various buildings, including tunnels [24,25]. For example, Hwang et al. [26] investigated the relationship between the critical ventilation velocity and the heat release rate in tunnel fires through CFD simulation. Aminzadeh et al. [27] numerically analyzed the temperature distributions for tunnel fires with different ventilation velocities and tunnel cross-sections. Wang et al. [28] validated the effectiveness of CFD tools in tunnel fire simulation by maintaining the same boundary conditions as the full-scale experiments. Zhang et al. [29] investigated the maximum ceiling temperature and the smoke back-layering length in a tilted tunnel under natural ventilation using CFD simulation. Gao et al. [30] numerically investigated the thermal smoke behavior and ceiling temperature distribution in a tilted tunnel through CFD simulation. Caliendo et al. [31] studied the risk reduction effect for tunnel fires equipped with a micronized water system by performing CFD modeling. Nishino et al. [32] investigated the effect of water sprays on the characteristics of smoke flow in tunnel fires through large eddy simulation. Wang et al. [33] considered different mechanical ventilation modes and fire locations to investigate the fire and smoke spreading characteristics in the natural gas cabin of urban underground utility tunnels based on CFD simulations. Fan et al. [34] considered the influence of unsteady piston wind and analyzed the characteristics of smoke motion for a burning subway train during emergency braking. Liu et al. [35] investigated the temperature distribution under the effect of ventilation durning a moving tunnel fire. These studies indicate the effectiveness of CFD tools in simulating fire combustion and fluid heat and mass transfer.

However, few studies have systematically investigated the combined effects of rainfall and fire in tunnels using CFD simulations. This study presents a CFD model for numerical simulations to investigate the dynamics of tunnel fires under heavy rainfall conditions. The accuracy of the proposed CFD model is initially validated using reduced-scale experimental data from previous studies [2–4]. Subsequently, full-scale tunnel fire simulations under rainfall conditions are performed to assess real-scale fire hazards. This study is pivotal in guiding the coupled modelling of rainfall and fire, thereby enhancing our understanding of multi-hazard risks in tunnel engineering. The findings of this study aim to contribute to the development of proactive strategies for enhancing tunnel safety and resilience in the face of increasing challenges posed by climatic changes and interconnected disaster scenarios.

2. Numerical methodology

2.1. Reference experiments

Numerical analyses presented in this paper are compared with the results of previously published experiments [2–4]. The fire tests were carried out on a small-scale (1:15) experimental platform, which included a model tunnel with dimensions of 10 m in length, 0.6 m in width, 0.4 m in height, and a rainfall simulator. A pool fire was positioned at the center of the tunnel. The artificial rainfall simulator, featuring adjustable rainfall intensity and raindrop size, was located on one side of the tunnel to evenly disperse raindrops through nozzles. Experiments included five rainfall intensities, three droplet size distributions, and three fire sizes. The temperature field within the experiment was mapped using 10 thermocouple trees with 11 K-Type 0.1 mm thermocouples, arranged symmetrically along the axis of the tunnel. Fig. 1 shows the diagram of the platform, including the locations of the rainfall simulator and thermocouples. More experimental details, results, and their analysis are available in previous studies [2,3]. Numerical simulation can be achieved through the coupled modeling of rainfall and tunnel fire.

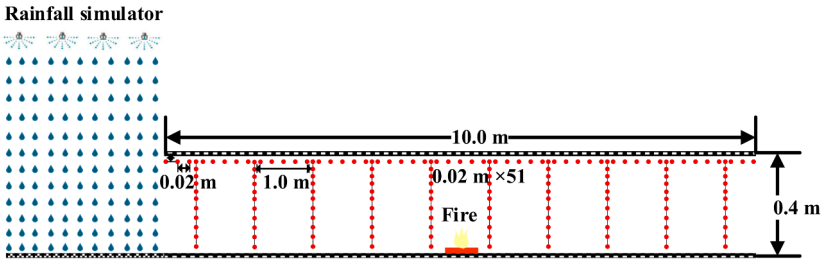

Fig. 1. Diagram of the experimental platform with rainfall simulator and thermocouple locations.

2.2. Rainfall simulation

The numerical simulation in this study is performed using ANSYS® Fluent 19.0. The simulation of raindrops is achieved by injecting water droplets from the top surface of the rain domain into the calculated flow pattern and further resolving their motion equations. There are two approaches to realize the rain simulation: Lagrangian Particle Tracking (LPT) and the Eulerian Multiphase (EM). LPT focuses on tracking the individual motion of particles suspended or immersed in a fluid flow. As a subset of LPT, the discrete phase model (DPM) specifically targets the modeling of discrete particles within a continuous phase. It treats raindrops as individual discrete particles, tracking each raindrop individually while considering its interaction with the surrounding airflow. This approach provides detailed information on raindrop dynamics. The EM approach considers raindrops as interpenetrating continua with space occupied, and raindrops of the same size are regarded as an independent phase. This approach provides a more macroscopic view of raindrop behavior in airflow but may not capture the detailed dynamics of individual raindrops.

The LPT method was employed in this study, considering the interaction between the air and raindrops. In addition to the momentum exchange with the air, the coupled heat-mass solution effects on the particles are set to their default values, with the vaporization limiting factors for mass and heat maintained at 0.3 and 0.1, respectively. The raindrops are assumed to be spheres of uniform size. The motion equation of a raindrop moving in a steady flow field is determined by the following equation, based on the Lagrangian Particle Tracking method:

$$m_d \frac{d\vec{u}_d}{dt} = m_d \frac{(\vec{u} - \vec{u}_d)}{\tau_r} + m_d \frac{\vec{g}\,(\rho_w - \rho)}{\rho_w} \tag{1}$$

where, m_d is the raindrop mass, kg; $\vec{u}$ is the air velocity, m/s; $\vec{u}_d$ is the raindrop velocity, m/s; $\vec{g}$ is the gravitational acceleration, m/s^2; ρ is the air density, kg/m^3; ρ_w is the raindrops density, kg/m^3; t is the time coordinat, s; τ_r is the droplet relaxation time calculated by:

$$\tau_r = \frac{\rho_w {d_0}^2}{18\mu} \frac{24}{C_D Re} \tag{2}$$

here, μ is the dynamic viscosity of air, N·s/m^2; d_0 is the raindrop diameter, m; C_D is the drag coefficient, Re is the relative Reynolds number, which is defined as

$$Re = \frac{\rho d_0 \left|\vec{u} - \vec{u}_d\right|}{\mu} \tag{3}$$

2.3. Tunnel fire simulation

This paper considers actual heat released in a single-step flame reaction for pool fire and adopts the mixed-controlled turbulent combustion model of species transport, enabling the calculation of multi-species transport. The Eddy-Dissipation Model (EDM) [36] is employed for turbulence-chemistry interaction, indicating the rapid combustion of fuels once mixed with the oxidizer. This approach, using a mixed-burned approximation, avoids complex Arrhenius chemical kinetics calculations and is acceptable for diffusion flames in pool fires. Selected fuel is the mixture material of ethyl-alcohol-air, and the fuel is introduced into the computational domain at a constant mass flow rate. The Moss-Brookes soot model is selected, and the mass of the incipient soot particle and the mean density of the soot particle remain at their default value of 144 kg/mol and 2000 kg/m^3. Ignition is achieved through a spark ignition model. The gas phase is treated as an ideal gas during combustion. Besides, the radiation is nonnegligible accounting for 30 % of the total heat loss in tunnel fires, and the Discrete Ordinate model (DO) is applied in this study. The tunnel wall is made of calcium-silicate boards, 0.02 m thick, with physical properties including a density of 2100 kg/m^3, a specific heat capacity of 880 J/(kg • K), and a thermal conductivity of 1.37 W/(m • K). A convective heat transfer coefficient of 20 W/(m^2 • K) and a diffuse fraction of 1 are specified for tunnel walls.

2.4. Computational domains and boundary conditions

The computational domain was modelled as two parts, corresponding to the rain domain and the tunnel domain, respectively. Fig. 2 shows the computational domains, boundary conditions, and coordinates of the numerical model. The dimensions of the tunnel are

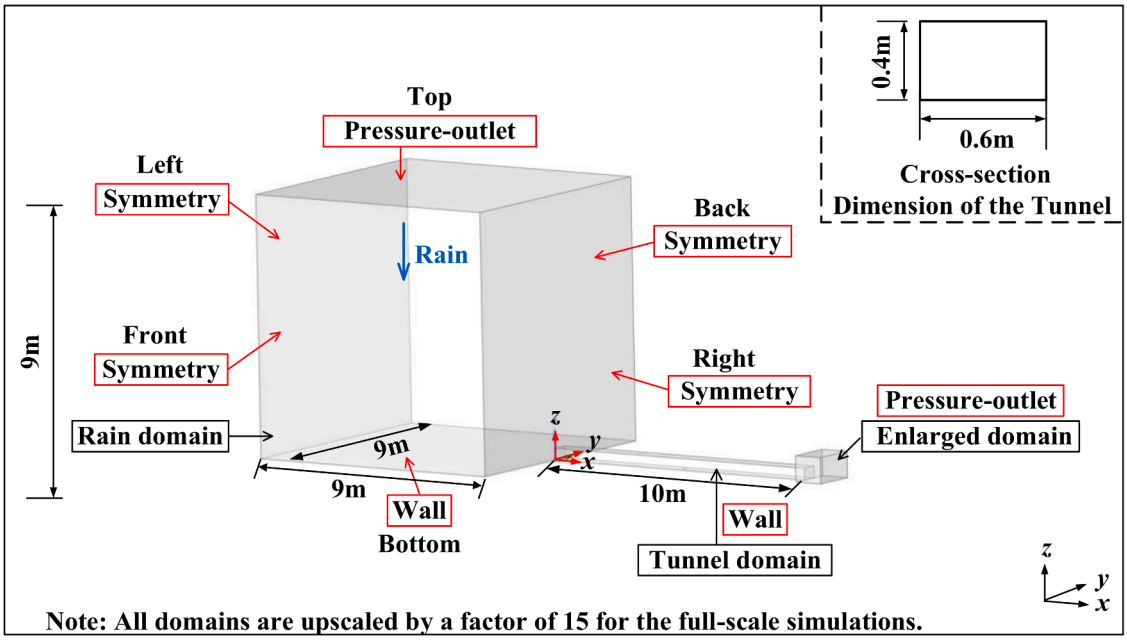

Fig. 2. Sketch of computational domains and boundary conditions.

10 m (length) × 0.6 m (width) × 0.4 m (height), consistent with the reduced-scale testbed [2–4]. To better simulate the rainfall weather, the rain domain is a much larger cube with a length of 9 m. The cross-sectional area ratio of the tunnel to the rain domain is about 0.3 %, and the height of the rain domain is about 18 times the hydraulic diameter of the tunnel section. The rain domain is sufficiently large to ensure the full development of turbulence. In addition, an enlarged computational domain is added at the other end of the tunnel, with a cross-section slightly larger than the tunnel. Previous studies [32,37] have shown that an enlarged computational domain favors simulating results as it eliminates the influence of boundary conditions. The same computational domain was used for the full-scale simulations, but upscaled by a factor of 15, with the origin in the same relative position to the domains.

The boundary conditions for the rain domain are set as follows.

- Both sides of the rain domain are set as symmetry,
- The top surface of the rain domain is set as a pressure-outlet with a gauge pressure of 0 Pa, and it also serves as the injection surface for the raindrops and air entrainment into the domain,
- The bottom of the rain domain is set as a no-slip wall,
- Inert raindrops are released from the top surface of the rain domain, and the release height ensures that they can reach their terminal velocity before entering the height of the tunnel domain,
- Raindrops are assigned a constant total flow rate, and the option to scale flow by face area is activated to ensure a uniform rainfall intensity,
- Raindrops are modelled as spheres of uniform diameter with an initial vertical velocity.

The boundary conditions for the tunnel domain are set as follows.

- Both sides of the tunnel domain are set as walls with roughness,
- The tunnel outlet is set as the pressure-outlet with a gauge pressure of 0 Pa.

Additionally, the ‘escape’ type is adopted for DPM conditions at the boundaries of the tunnel domain and the rain domain. This means that raindrops leave the domain as soon as they hit the boundary surface, and complex phenomena such as splashing, bouncing, and evaporation are neglected. The enlarged domain boundaries are all set as the pressure-outlets with a gauge pressure of 0 Pa. Share coincident topology is used to establish connections between the three domains.

2.5. Solution strategy and solve setting

The computational mesh adopts polyhedral cells. The grid for the tunnel domain is refined locally, while the grid for the rain domain is coarser to optimize computational resources. In cases involving fire, the mesh for the fire plume is further refined. The grid size of the enlarged domain remains the same as the rain domain. To ensure that the grid density did not affect the calculation results, a grid independence analysis is necessary.

There are multiple options for turbulence models, such as the RANS (Reynolds Averaged Navier-Stokes) model and the LES (Large-eddy simulation) model. Each model has its limitations and advantages. The RANS approach involves a statistical treatment of time-averaged unsteady flow, which has advantages in computational efficiency and can provide reasonable predictions for many large-

scale model applications, especially when the flow is predominantly turbulent and separation effects are not dominant [38]. The $k-\varepsilon$ model is the most commonly used RANS approach due to its efficient calculation and wide applicability.

For the LES approach, the Navier-Stokes equations are filtered in space. This filtering enables accurate resolution of scales larger than the grid using a space-time scheme, while modeling turbulence with smaller scales. It is well-suited for capturing unsteady and complex turbulent flows, including separated and swirling flows [39]. However, LES is computationally expensive, especially for high Reynolds number flows or complex geometries, requiring fine grid resolution to capture small-scale turbulence. It is recommended [28,40] that the grid size (δ_x) meets $D^*/\delta_x \in [4,16]$ to obtain good results in simulations. Here, D^* is the characteristic diameter of the fire, which can be calculated as follows:

$$D^* = \left(\frac{\dot{Q}}{\rho c_p T_0 \sqrt{g}}\right)^{(2/5)} \tag{4}$$

where, $\dot{Q}$ is the heat release rate, kW; T_0 is the ambient temperature, K; ρ is the air density, kg/m^3; and c_p is the specific heat capacity of air, kJ/kg • k. The grid sizes of the tunnel and fire selected in this study are within the recommended range.

To simulate incompressible turbulent flow, two turbulent models, Realizable $k-\varepsilon$ and Algebraic Wall-Modelled LES Model (WM-LES), are used in this study. The pressure-velocity coupling is solved using the algorithm of the Semi-Implicit Method for Pressure-Linked Equations (SIMPLE), and the pressure equations are discretized using the Body Force Weighted scheme. The momentum equations are solved using the second-order upwind spatial discretization scheme. Second-order discretization schemes are also applied to the density terms and energy terms. Under-relaxation coefficients adopt ANSYS® Fluent default values. The physical sub-models and the initial boundary conditions are listed in Table 1. The simulation was conducted with a total number of time steps of 6000, with the time step size set to 0.1 s, resulting in a total simulated period of 600 s.

Three meshes (coarse, medium, and fine) are generated using the same meshing strategy, as shown in Table 2. The induced airflow velocity distributions and the ceiling excess temperature distributions under three mesh sizes using the turbulent model of "Realizable $k-\varepsilon$ model, enhanced wall functions" are shown in Fig. 3. It can be found that results from the medium mesh and the fine mesh do not show significant differences. Considering the accuracy of simulation results and the economy of computational resources, the medium grid, consisting of a total of 636,562 cells, is chosen. Ultimately, unstructured polyhedral meshes with a size of 0.01 m are employed in the fire area, meshes with a size of 0.02 m are used in the tunnel domain, and meshes with a maximum cell length of 0.3 m are used in the rain domain and the enlarged domain. Besides, the implementation of FLUENT's automatic wall treatment is adopted, with boundary layer mesh settings that include a transition ratio of 0.272, three layers, and a growth rate of 1.2, allowing for adaptive mesh refinement. In Fig. 4, the mesh scheme of the model is presented.

3. Modelling results and validation

3.1. Raindrop terminal velocity and determination of rainfall domain height

In the process of raindrops falling, their motion is primarily influenced by gravity, drag, and buoyancy. As the subjected forces reach a balance, raindrops fall at a constant terminal velocity (V_t). Fig. 5 shows velocity variation along the path for a single raindrop released from a height of 20 m with an initial vertical velocity (V_0) for different raindrop sizes (d_0). It can be observed that the terminal velocity of raindrops is solely determined by their size. For raindrop sizes of 1.0 mm, 1.2 mm, and 1.5 mm, the corresponding ter-

Table 1
Setting of sub-models and initial conditions.

Sub-models	Simulation parameters
Solver	Pressure-based
Time	Transient
Turbulent model	Realizable $k-\varepsilon$, LES
Computational scheme	SIMPLE
Radiation heat-transfer sub-model	Discrete Ordinates
Soot model	Moss-Brookes
External air and wall temperature	300 K
Operating pressure	101,350 Pa
Gravity	−9.81 m/s^2

Table 2
Setting of the three mesh sizes.

Domains	Coarse mesh	Medium mesh	Fine mesh
Tunnel domain	0.025 m	0.02 m	0.015 m
Fire domain	0.01 m	0.01 m	0.01 m
Rain domain	0.40 m	0.30 m	0.25 m
Enlarged domain	0.40 m	0.30 m	0.25 m
Total cell	345,627	624,925	1,352,948
Consumption time	8 h	14 h	30 h

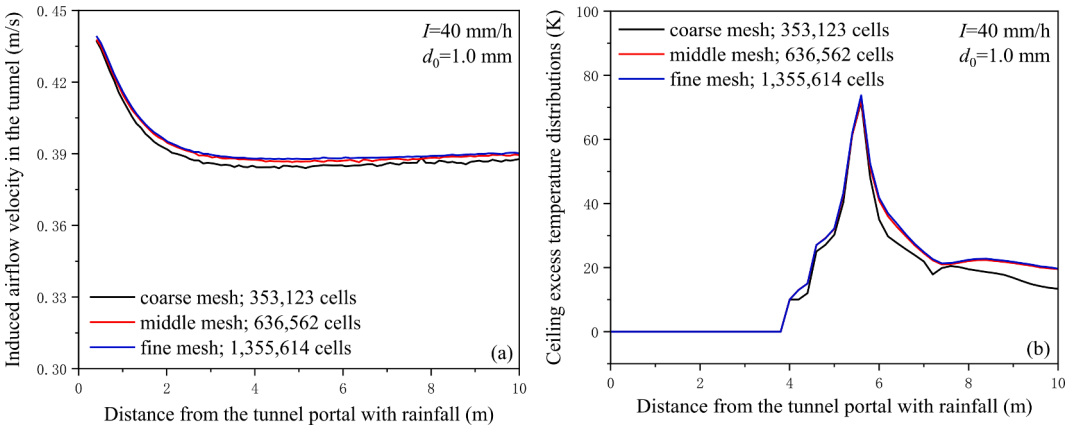

Fig. 3. Results of mesh independence analysis (a) Velocity distribution of the induced airflow in the tunnel; (b) Excess temperature distribution beneath the tunnel ceiling.

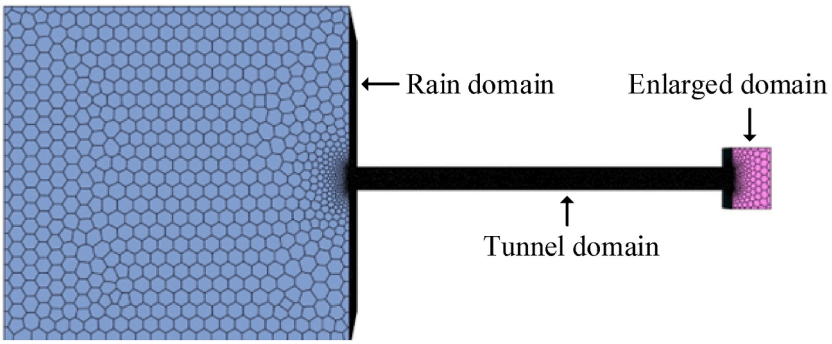

Fig. 4. Mesh scheme of the model.

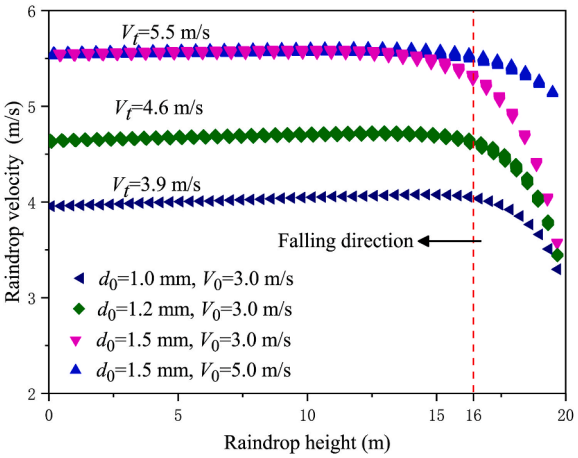

Fig. 5. Variation of velocity along the path for a single raindrop.

minal velocities are 3.9 m/s, 4.6 m/s, and 5.5 m/s, respectively. When raindrops of the same size are given different initial velocities, their terminal velocities remain the same, and only the path length required to reach balance differ. The smaller the difference between the initial velocity and terminal velocity, the shorter the path length the raindrop travels to reach balance. For instance, when the initial velocity of raindrops is 3 m/s, raindrops for three varied sizes reach their terminal velocity after traveling a distance about 4 m.

It is worth noting that terminal velocities of raindrops obtained from the simulation are slightly smaller than the results of the theoretical analysis in Ref. [2]. Specifically, the terminal velocities of raindrops with sizes of 1.0 mm, 1.2 mm, and 1.5 mm are 4.64 m/s, 5.09 m/s, and 5.69 m/s, respectively. The reason is that the air buoyancy raindrops subjected is ignored in theoretical analysis. Besides, considering the fluid obstruction ratio, i.e., the ratio of tunnel height to rain-domain height is less than 5 %, and taking into ac-

count the turbulence development of raindrops, the rain domain with a height of 9 m is sufficient when the initial release velocity of droplets is set as 3 m/s. This allows the raindrops to reach the terminal velocity before falling into the tunnel height.

3.2. Rainfall induced flow field and model validation

Continuous raindrops increase local pressure of rain domain, creating a pressure difference between both ends of the tunnel. In Fig. 6, the pressure distribution at the half height of the tunnel (see Fig. 6(a), slices of $z = 0.2$ m) and the pressure distribution at the tunnel portal with rainfall (see Fig. 6(b), slices of $x = 0$ m) under different rainfall conditions are shown. It is observed that there is a positive pressure difference between the tunnel end with rainfall and the no-rainfall tunnel end. This pressure difference increases with increasing rainfall intensity while decreases with increasing raindrop size. The simulated values and theoretical analysis [2] of the increased local pressure are presented in Table 3, and the small deviation indicates the accuracy of the simulation.

Taking the case of $I = 40$ mm/h and $d_0 = 1.0$ mm as an example, the tunnel flow field induced by rainfall is shown in Fig. 7(a). It can be found that the pressure difference caused by rainfall generates a longitudinal flow field inside the tunnel, with the airflow directed from the tunnel end with rainfall to the no-rain tunnel end. The airflow velocity along the longitudinal centerline, measured at half height of the tunnel, is monitored. A comparison between the simulation results and the velocity distributions recorded at the same locations in the model test [2,3] is shown in Fig. 7(b). The simulation results of the velocity distribution show a strong correlation with the experimental findings when considering a roughness height of 0.025 m and a roughness constant of 1.0 for tunnel walls. However, the velocity decay of the induced airflow along the tunnel in the experiment is more pronounced than in the simulations. There are two potential reasons: one is the energy loss caused by thermocouple trees, and the other is the additional drag due to increased air humidity caused by fog entering the tunnel.

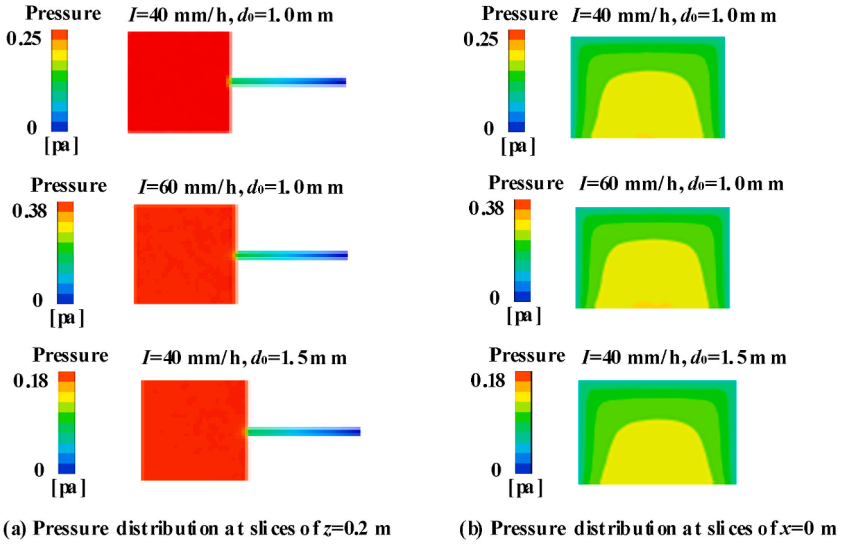

Fig. 6. Pressure distribution at (a) slices of $z = 0.2$ m and (b) slice of $x = 0$ m under different rainfall conditions.

Table 3
Increased local ambient pressure at the tunnel portal with rainfall.

Rainfall intensity I (mm/h)	Raindrop size d_0 (mm)	Simulation value ΔP_s (pa)	Theoretical value ΔP_t (pa)	Deviation $(\Delta P_s - \Delta P_t)/\Delta P_t$
20	1.0	0.1188	0.1197	−0.75 %
	1.2	0.1010	0.1092	−7.51 %
	1.5	0.0847	0.0977	−13.30 %
30	1.0	0.1783	0.1795	−0.67 %
	1.2	0.1517	0.1639	−7.44 %
	1.5	0.1271	0.1466	−13.30 %
40	1.0	0.2380	0.2393	−0.54 %
	1.2	0.2004	0.2185	−8.28 %
	1.5	0.1698	0.1954	−13.10 %
50	1.0	0.2975	0.2992	−0.57 %
	1.2	0.2531	0.2731	−7.32 %
	1.5	0.2123	0.2443	−13.10 %
60	1.0	0.3571	0.3590	−0.53 %
	1.2	0.3038	0.3277	−7.29 %
	1.5	0.2548	0.2931	−13.07 %

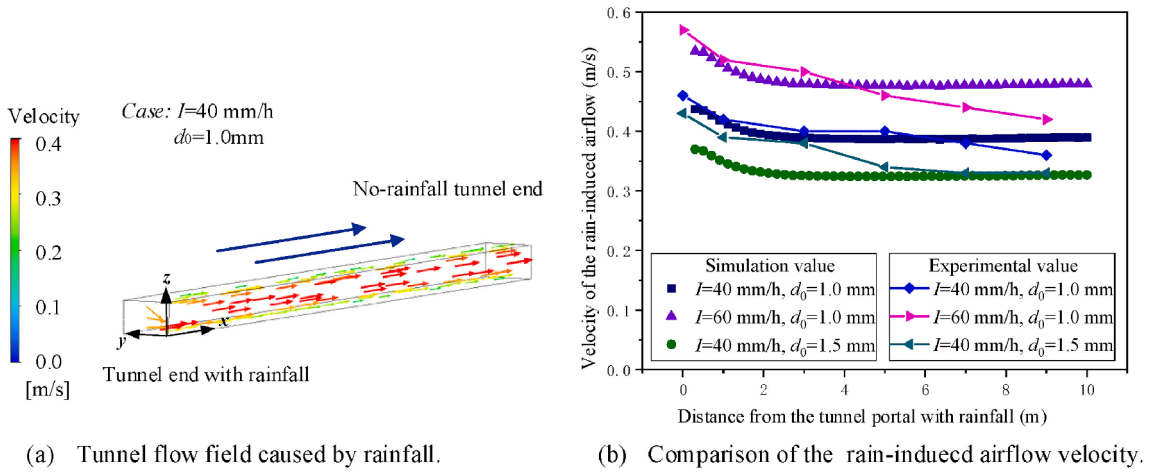

Fig. 7. (a) Flow field structure and (b) velocity distribution inside the tunnel caused by rainfall.

3.3. *Modelling reduced-scale tunnel fire under rainfall condition*

The fire source is positioned at the center of the tunnel with a side length of 8 cm, and the fuel inlet is set as a mass flow inlet with a stable rate, following the stable mass burning rate in the experimental tests [2–4]. The heat release rate is about 2.2 kW–2.6 kW under different rainfall conditions, equivalent to 2.0 MW–2.3 MW in real-scale tunnel fires. To simplify the simulation and save computational resources, the following basic assumptions are followed: 1) the temperature (T_0) in the tunnel is uniform before the fire occurs; 2) the ventilation airflow and smoke generated by the fire are considered as ideal gases; and 3) the temperature on the outer wall of the tunnel is the same as the ambient temperature and remains constant during a fire.

This study compares two turbulent models: the "Realizable $k-\varepsilon$ model, enhanced wall functions" and the LES model. The calculation time (t) lasts 600 s, and the fuel combustion and smoke movement reach a steady state at around 200 s. Fig. 8(a) and Fig. 8(b) show the HRR (Heat Release Rate) profiles of fires and stable fire plumes under no rainfall conditions, respectively, using the two turbulence models. It can be observed that the LES model can capture the transient puffing behavior [41] that is inherent to turbulent pool fires, while the RANS model gives a steady HRR over time due to its time-averaged treatment method. Regarding fire plumes, the LES model can capture small eddies more effectively than the RANS model.

The temperature distribution at the tunnel ceiling is crucial in tunnel fire research, as it directly impacts fire spread, smoke movement, and the safety of tunnel structures and occupants. Fig. 9(a) shows the computational gas excess temperature distribution beneath the tunnel ceiling under no rainfall conditions at $t = 600$ s with the two turbulent models, considering heat transfer from tunnel walls. It is observed that the results of maximum ceiling gas temperature and temperature distribution both exhibit discrepancies between the RANS and LES models. In addition, there is a lower temperature area near the fire source in the LES model results, possibly due to a special phenomenon known as "hydraulic jump" in fluid flow, which is characterized by a sudden decrease in energy.

The gas temperature (T_g) from CFD simulations is always higher than the value measured in the experiments as obtained by the thermocouple (T_{tc}). Due to radiation heat loss, the thermocouple bead will never be heated to the true temperature of the hot gas, and such a deviation becomes larger for a large thermocouple bead [42–44]. In FDS, this can be compensated by the introduction of the 'THERMOCOUPLE' device, which represents a modelled thermocouple. Warzynski et al. [45] studied in detail the temperature compensation in CFD code and referred to it as the thermocouple model. The thermocouple temperature in a fire test can be obtained from

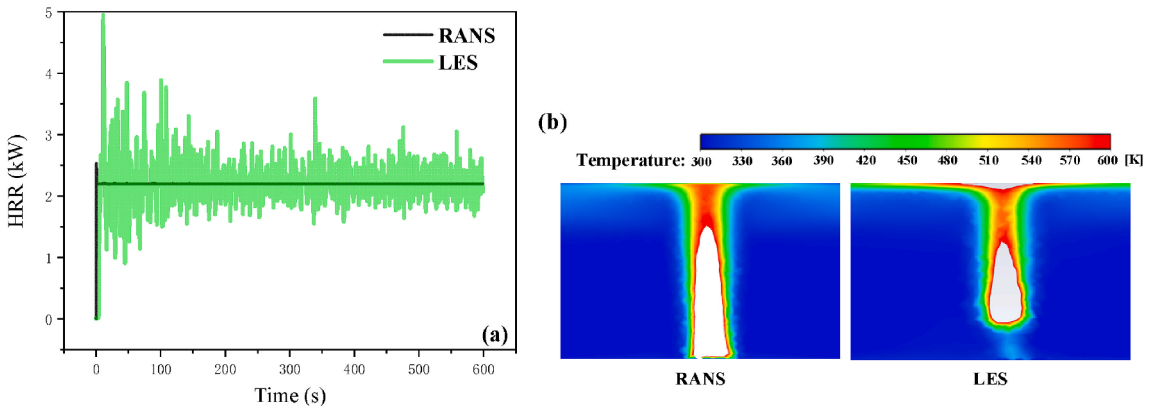

Fig. 8. Comparison of (a) HRR profiles and (b) fire plumes with different turbulent models.

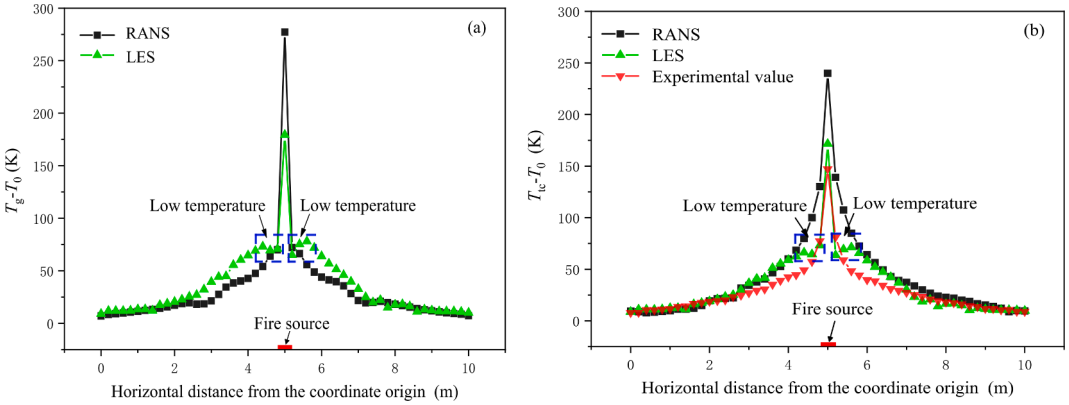

Fig. 9. Ceiling excess temperature under no rainfall conditions (a) Computational gas temperature with different turbulent models, and (b) Comparison between the modelled thermocouple temperature data and the experimental data.

gas temperature by solving the equation in the Appendix. Fig. 9(b) shows the comparison between the modelled thermocouple ceiling excess temperature based on the thermocouple model and the experimental data [2,3], where it can be found that both turbulent models tend to overpredict the ceiling temperature, especially near the fire source. However, the LES model has a better prediction of maximum ceiling temperature than the RANS model.

When the DPM model is activated, raindrops play a significant role in the flow pattern. The rain-induced airflow prevents the spread of smoke to the rainfall tunnel portal. In Fig. 10, the ceiling excess temperature from the thermocouple model under different rainfall conditions is compared with the experimental data [2,3]. The results of both turbulent models show good prediction in terms of the smoke back-layer length. However, the RANS model has better performance in predicting ceiling temperature distributions. From Figs. 9 and 10, it can be observed that the LES model provides a better prediction of temperature distribution for tunnel fires in the absence of rainfall, while the RANS model performs better for tunnel fires in the presence of rainfall in the current model setup.

3.4. Modelling full-scale tunnel fires and scale analysis

A scale factor of $\gamma = 15$ is used to scale up the model to real tunnel size, with dimensions of 150 m (length) × 9 m (width) × 6 m (height). Numerical simulations of full-scale tunnel fires under equivalent rainfall boundary conditions and fire sizes are performed based on the Froude similarity criterion. Table 4 lists the significant scale correlations for the Froude similarity criteria. It is worth noting that the thermal properties of the tunnel wall are not included in the scaling relationship because it is impossible to keep all forms of heat transfer constant in fire simulations [46]. A wall thickness of 20 cm has been proven to provide a reasonable prediction in full-scale tunnel fire simulations [47].

Table 5 presents the equivalent rainfall conditions and fire sizes for the two cases in Fig. 10 based on the scaling correlations of the Froude similitude criterion. The modelled thermocouple temperature distributions beneath the tunnel ceiling for equivalent full-scale tunnel fires, calculated using the RANS turbulent model, are also shown in Fig. 10 with star symbols, where the distance from the rainfall tunnel portal corresponds to the small-scale scenario. It can be found that the temperature distribution follows the scaling relationship between different fire scales. The maximum excess temperature of the full-scale tunnel fires is slightly lower than experimental and small-scale tunnel fires, possibly due to scaling deviations in the heat transfer of tunnel walls.

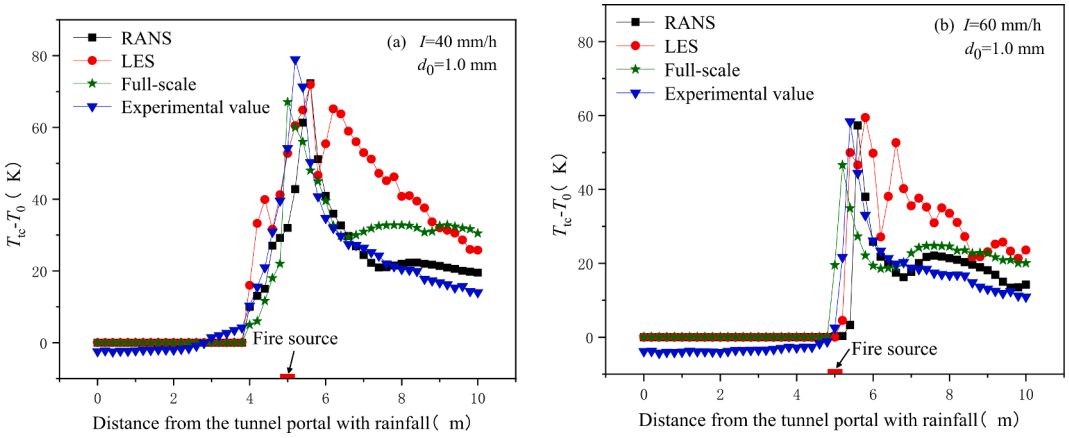

Fig. 10. Comparison of ceiling excess temperature between the simulation and experimental under different rainfall conditions (a) $I = 40$ mm/h, $d_0 = 1.0$ mm, and (b) $I = 60$ mm/h, $d_0 = 1.0$ mm.

Table 4
Scaling correlations of the Froude similitude criterion.

Parameters	Symbol	Scaling correlations
Length	L [m]	$L_{full} = \gamma L_{model}$
Heat release rate	Q [kW]	$Q_{full} = \gamma^{5/2} Q_{model}$
Rainfall intensity	I [mm/h]	$I_{full} = \gamma^{1/2} I_{model}$
Raindrop size	d_0 [mm]	$d_{0full} = \gamma^{1/2} d_{0model}$
Mass flow rate	$\dot{m}$ [kg/s]	$\dot{m}_{full} = \gamma^{5/2} \dot{m}_{model}$
Pressure	P [pa]	$P_{full} = \gamma P_{model}$
Velocity	u [m/s]	$u_{full} = \gamma^{1/2} u_{model}$
Temperature	T [K]	$T_{full} = T_{model}$
Time	t [s]	$t_{full} = \gamma^{1/2} t_{model}$

Table 5
Equivalent rainfall condition and fire size in small-scale and full-scale simulation.

Parameters	Small-scale	Full-scale
Rainfall intensity	40 mm/h, 60 mm/h	155 mm/h, 232 mm/h
Raindrop size	1.0 mm	3.87 mm
Heat release rate	2.2 kW, 2.6 kW	2.0 MW, 2.3 MW
Mass flow rate	0.083 g/s, 0.096 g/s	0.072 kg/s, 0.084 kg/s

The above analysis indicates that the current model setup can effectively simulate full-scale tunnel fires under the influence of rainfall. For instance, tunnel fires with rainfall intensities of 100 mm/h, 150 mm/h, and 200 mm/h, as well as raindrop diameters of 4 mm and 6 mm, have been numerically investigated. The induced airflow velocity in the tunnel under different rainfall conditions is shown in Fig. 11. Table 6 lists the information on the increased local pressures and the maximum velocities of the induced airflow under different rainfall conditions.

To investigate the relationship between the increased local pressures and the maximum induced airflow velocities with rainfall parameters, data from all simulation cases, including the reduced-scale cases in Table 5 and the full-scale cases, are analyzed. Fig. 12(a) and (b) show the relationship between the increased local pressures and the maximum induced airflow velocities with rainfall para-

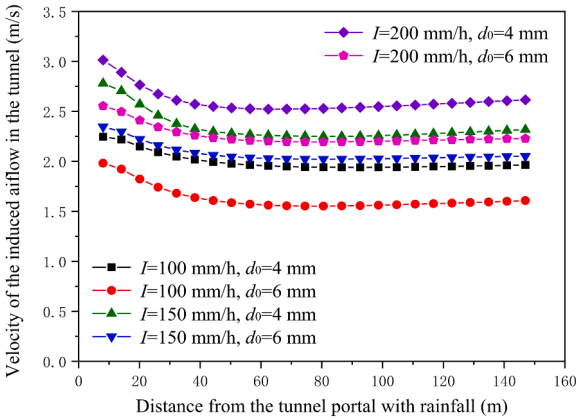

Fig. 11. Induced airflow velocity under different rainfall conditions.

Table 6
Information of the increased local pressures and the maximum induced airflow velocities under different rainfall conditions.

Rainfall intensity I (mm/h)	Raindrop size d_0 (mm)	Increased pressures ΔP (pa)	Maximum velocity u_{max} (m/s)
100	4	3.5945	2.25
	6	2.7709	1.98
150	4	5.2356	2.78
	6	4.2523	2.35
200	4	6.8102	3.01
	6	5.4673	2.55

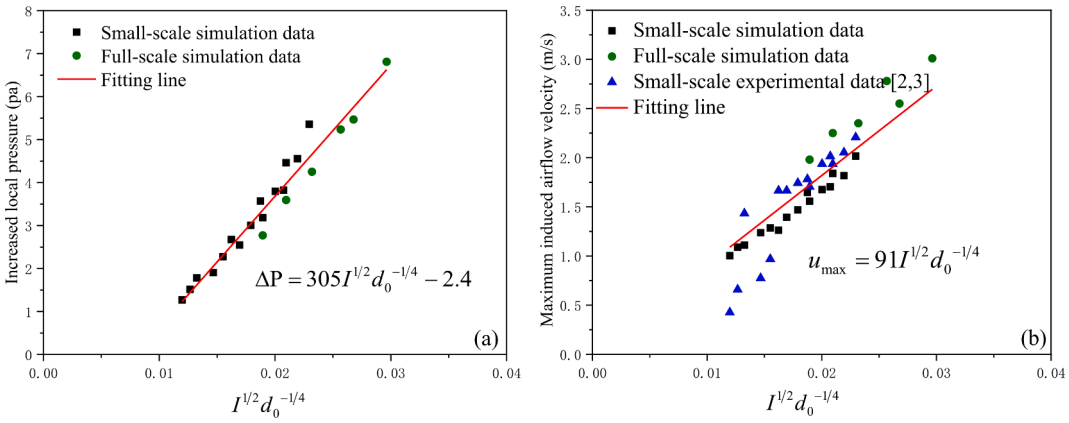

Fig. 12. Relationship between the (a) increased local pressure and the (b) maximum induced airflow velocity and the rainfall parameters.

meters, respectively, maintaining the data in equivalent full-scale, in SI units. Consequently, Eq. (5) and Eq. (6) can be used to predict the increased local pressure and the maximum induced airflow velocity under the influence of rainfall, respectively.

$$\Delta P = 305 I^{1/2} d_0^{-1/4} - 2.4 \tag{5}$$

$$u_{max} = 91 I^{1/2} d_0^{-1/4} \tag{6}$$

The fuel is introduced from the center of the tunnel with an area of 1.44 m^2 at a steady mass flow rate of 0.08 kg/s, using ethyl-alcohol-air as the fuel, and the calculated heat release rate is about 2.25 MW, representing a car fire. Fig. 13 shows the temperature field and velocity field at steady state under different rainfall conditions. The rainfall-induced airflow limits the smoke back-layering toward the rainfall portal and accelerates the smoke spread toward the no-rainfall portal. As a result, the height of the smoke layer near the no-rainfall portal decreases, which hinders evacuation and rescue efforts. Tunnel fire dynamics under rainfall effect deserve more attention.

4. Conclusions

This study presents a computational fluid dynamics (CFD) model for investigating the dynamics of tunnel fires under heavy rainfall conditions. The model was validated against model-scale tests, showing good agreement with experimental results. Subsequently, full-scale tunnel fires under rainfall conditions were modelled, effectively predicting the temperature field and smoke motion. The main findings are as follows.

(1) Discrete phase model based on the Lagrangian approach shows excellent performance in rainfall simulation, while the species transport model effectively captures pool fire combustion. The interaction between fires and rainfall is addressed by considering the interplay between the discrete phase and continuous phases. Large Eddy Simulation (LES) model provides better predictions of temperature distribution for tunnel fires in the absence of rainfall, while Reynolds Averaged Navier-Stokes (RANS) model performs better under rainfall conditions in the current model setup.

(2) A positive pressure difference exists between the tunnel end exposed to rainfall and the tunnel end without rainfall, inducing longitudinal airflow within the tunnels. This rain-induced airflow prevents smoke from reaching the tunnel end

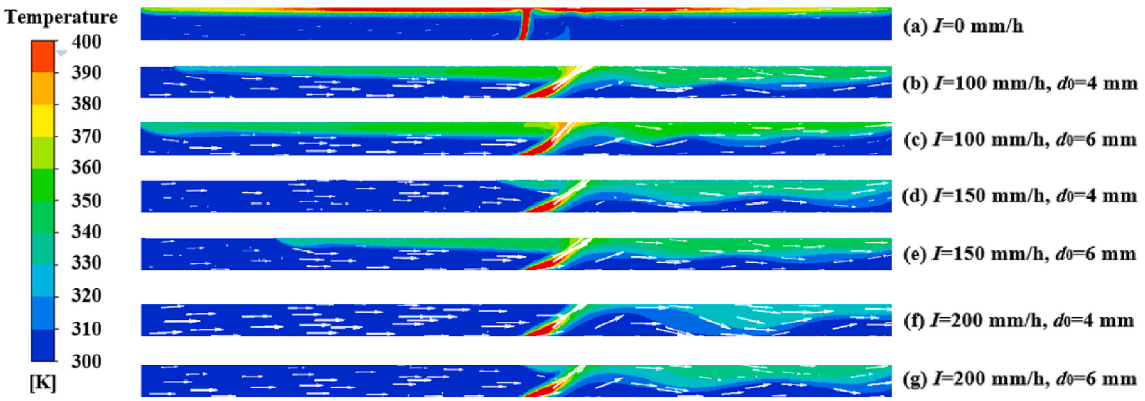

Fig. 13. Temperature field and velocity field under different rainfall conditions.

exposed to rainfall and decreases smoke height near the tunnel end without rainfall. Furthermore, the gas temperature predicted by CFD simulations consistently exceeds the values measured by thermocouples. Incorporating a thermocouple model could help reduce this overprediction.

(3) This study is pivotal in guiding the coupled modeling of rainfall and fire, enhancing our understanding of multi-hazard risks in tunnel engineering. However, it is crucial to acknowledge that this study focuses solely on the impact of rainfall on tunnel fires, without considering the effects of natural wind. Future research will investigate the dynamic characteristics of tunnel fires in wind-driven rain environments to improve the comprehensive understanding under extreme weather conditions.

CRediT authorship contribution statement

Dia Luan: Writing – original draft, Methodology, Investigation. **Jakub Bielawski:** Writing – review & editing, Methodology. **Chuangang Fan:** Supervision, Resources, Funding acquisition. **Wojciech Węgrzyński:** Writing – review & editing. **Xinyan Huang:** Conceptualization, Funding acquisition, Supervision, Writing – review & editing.

Declaration of competing interest

The authors declare that they have no known competing financial interests or personal relationships that could have appeared to influence the work reported in this paper.

Acknowledgments

This work is supported by National Natural Science Foundation of China (Grant No. 52278545), the Key Research and Development Program of Hunan Province (Grant No. 2022SK2093), the Natural Science Foundation of Hunan Province of China (Grant No. 2024JJ2075), Central South University Research Programme of Advanced Interdisciplinary Studies (Grant No. 2023QYJC024), and Hong Kong Research Grants Council Theme-based Research Scheme (T22-505/19-N). The authors are grateful for resources from the High-Performance Computing Center of Central South University.

Data availability

Data will be made available on request.

Appendix

Thermocouple Model:

Comparison of experimental and numerical data is challenged by the differences in temperature measured by thermocouples (devices that have its own thermal properties and bulk) and the gas phase temperature reported in CFD. The thermocouple temperature (T_{tc}) [48] in the fire test can be determined by solving the following equation,

$$\frac{D_{tC}}{6}\rho_{tc}C_{tc}\frac{dT_{tc}}{dt} = \varepsilon_{tc}\left(\frac{U}{4} - \sigma {T_{tc}}^4\right) + h\left(T_g - T_{tc}\right) \tag{7}$$

where, D_{tc}, ρ_{tc}, C_{tc}, and ε_{tc} are the bead diameter, bead density, the specific heat, and the emissivity of the thermocouple, respectively. U is the integrated radiative intensity, T_g is the true gas temperature.

The convective heat transfer coefficient (h) of a small sphere decreases with the increasing diameter as

$$h = kNu/D_{tc} \tag{8}$$

$$Nu = 0.42\ Pr^{0.2} + 0.57\ Pr^{0.33}Re^{0.5}, Pr = \frac{\mu C_p}{k}, Re = \frac{\rho v D_{tc}}{\mu} \tag{9}$$

where, Nu, Pr, and Re are the Nusselt number, the Prandtl number and the Reynolds number, respectively. μ, c_p, k, and v are the dynamic viscosity, the specific heat, the thermal conductivity, and the fluid velocity, which are 1.85×10^{-5}(N • s/m^2), 1.007 kJ/(kg • K), 0.0263 W/(m • K), and 1.59×10^{-5}(m^2/s) for air at atmospheric pressure, respectively. If the thermocouple is nickel, the emissivity, bead density and specific heat are 0.85, 8908 kg/m^3 and 0.44 kJ/(kg • K), respectively [49]. The bead diameter in experiment was 0.001 m [2,3]. Then, the modelled thermocouple temperature can be calculated to compare with experimental measurements.

References

[1] Meteorological Bureau of Shenzhen Municipality, Shenzhen climate bulletin 2023, 26 JanChinese. http://weather.sz.gov.cn/, 2024.
[2] C. Fan, D. Luan, R. Bu, Z. Sheng, F. Wang, X. Huang, Can heavy rainfall affect the burning and smoke spreading characteristics of fire in tunnels? Int. J. Heat Mass Transf. 207 (2023) 123972.
[3] D. Luan, R. Bu, Z. Sheng, C. Fan, X. Huang, Experimental study on the impact of asymmetric heavy rainfall on the smoke spread and stratification dynamics in tunnel fires, Tunn. Undergr. Space Technol. 134 (2023) 104992.
[4] D. Luan, J. Bielawski, C. Fan, W. Węgrzyński, X. Huang, Impact of rainfall on smoke dynamics in longitudinally ventilated tunnels: model-scale fire test study, J. Therm. Anal. Calorim. Accept (2024).
[5] W. Węgrzyński, G. Krajewski, Influence of wind on natural smoke and heat exhaust system performance in fire conditions, J. Wind Eng. Ind. Aerodyn. 164 (2017) 44–53.

[6] W. Węgrzyński, G. Krajewski, P. Suchy, T. Lipecki, The influence of roof obstacles on the performance of natural smoke ventilators in wind conditions, J. Wind Eng. Ind. Aerodyn. 189 (2019) 266–275.
[7] W. Węgrzyński, T. Lipecki, Wind and fire coupled modelling—Part I: literature review, Fire Technol. 54 (2018) 1405–1442.
[8] W. Węgrzyński, T. Lipecki, G. Krajewski, Wind and fire coupled modelling—Part II: good practice guidelines, Fire Technol. 54 (2018) 1443–1485.
[9] H. Kataoka, Y. Ono, K. Enoki, Applications and prospects of CFD for wind engineering fields, J. Wind Eng. Ind. Aerodyn. 205 (2020) 104310.
[10] M. Shirzadi, M. Naghashzadegan, P.A. Mirzaei, Improving the CFD modelling of cross-ventilation in highly-packed urban areas, Sustain. Cities Soc. 37 (2018) 451–465.
[11] B. Blocken, J. Carmeliet, Validation of CFD simulations of wind-driven rain on a low-rise building facade, Build. Environ. 42 (2007) 2530–2548.
[12] A. Kubilay, D. Derome, B. Blocken, J. Carmeliet, Wind-driven rain on two parallel wide buildings: field measurements and CFD simulations, J. Wind Eng. Ind. Aerodyn. 146 (2015) 11–28.
[13] X. Gao, Z. Yang, D. Han, K. Gao, Q. Zhu, The impact of wind on the rainfall-runoff relationship in urban high-rise building areas, Hydrol. Earth Syst. Sci. 25 (2021) 6023–6039.
[14] H. Wang, X. Hou, Y. Deng, Numerical simulations of wind-driven rain on building facades under various oblique winds based on Eulerian multiphase model, J. Wind Eng. Ind. Aerodyn. 142 (2015) 82–92.
[15] H. Wang, W. Song, Y. Chen, Numerical simulation of wind-driven rain distribution on building facades under combination layout, J. Wind Eng. Ind. Aerodyn. 188 (2019) 375–383.
[16] H. Wang, Q. Zhou, Field measurement and numerical simulation on distribution characteristics of wind-driven rain in setback buildings, J. Build. Eng. 72 (2023) 106686.
[17] M. Liu, S.H. Huang, B.W. Yan, Q.S. Li, Modelling of turbulent dispersion for numerical simulation of wind-driven rain on bridges, Environ. Fluid Mech. 18 (2018) 1463–1489.
[18] J. Llarena, L. Cabezuelo, A. Bilbao, Application of CFD simulations of wind-driven rain (WDR) on the new roof extension for San Mames new football stadium, J. Wind Eng. Ind. Aerodyn. 178 (2018) 105–111.
[19] M. Yu, J. Liu, Z. Dai, Aerodynamic characteristics of a high-speed train exposed to heavy rain environment based on non-spherical raindrop, J. Wind Eng. Ind. Aerodyn. 211 (2021) 104532.
[20] D.-H. Ouyang, E. Deng, Y.-Q. Ni, W.-C. Yang, Z.-W. Chen, Evolution of flow field around high-speed trains meeting at the tunnel entrance under strong wind-rain environments, J. Wind Eng. Ind. Aerodyn. 241 (2023) 105537.
[21] D. Wang, L. Li, J.W.Z. Lu, A.Y.T. Leung, V.P. Iu, K.M. Mok, Efficient meshfree large deformation simulation of rainfall induced soil slope failure, in: Hong Kong-Macau (China), 2010, pp. 662–667.
[22] A. Fávero Neto, A. Askarinejad, S. Springman, R. Borja, Simulation of debris flow on an instrumented test slope using an updated Lagrangian continuum particle method, Acta Geotech. 15 (2020) 2757–2777.
[23] E. Zehe, C. Jackisch, A Lagrangian model for soil water dynamics during rainfall-driven conditions, Hydrol. Earth Syst. Sci. 20 (2016) 2511–3526.
[24] L. Hu, N. Fong, L. Yang, W. Chow, Y. Li, R. Huo, Modeling fire-induced smoke spread and carbon monoxide transportation in a long channel: fire Dynamics Simulator comparisons with measured data, J. Hazard Mater. 140 (2007) 293–298.
[25] T. Baalisampang, E. Saliba, F. Salehi, V. Garaniya, L. Chen, Optimisation of smoke extraction system in fire scenarios using CFD modelling, Process Saf. Environ. Prot. 149 (2021) 508–517.
[26] C.C. Hwang, J.C. Edwards, The critical ventilation velocity in tunnel fires—a computer simulation, Fire Saf. J. 40 (2005) 213–244.
[27] A. Amouzandeh, M. Zeiml, R. Lackner, Real-scale CFD simulations of fire in single- and double-track railway tunnels of arched and rectangular shape under different ventilation conditions, Eng. Struct. 77 (2014) 193–206.
[28] Y.F. Wang, T. Qin, X.F. Sun, S. Liu, J.C. Jiang, Full-scale fire experiments and simulation of tunnel with vertical shafts, Appl. Therm. Eng. 105 (2016) 243–255.
[29] X. Zhang, Numerical Simulation on the Maximum Temperature and Smoke Back-Layering Length in a Tilted Tunnel under Natural Ventilation, 2021.
[30] Z. Gao, L. Li, C. Sun, W. Zhong, C. Yan, Effect of longitudinal slope on the smoke propagation and ceiling temperature characterization in sloping tunnel fires under natural ventilation, Tunn. Undergr. Space Technol. 123 (2022) 104396.
[31] C. Caliendo, G. Genovese, I. Russo, A numerical study for assessing the risk reduction using an emergency vehicle equipped with a micronized water system for contrasting the fire growth phase in road tunnels, Appl. Sci. 11 (2021) 5248.
[32] R. Nishino, N. Ren, Y. Noda, F. Tanaka, Large eddy simulation of smoke blocking by water sprays in a tunnel fire, Tunn. Undergr. Space Technol. 121 (2022) 104278.
[33] W. Wang, Z. Zhu, Z. Jiao, H. Mi, Q. Wang, Characteristics of fire and smoke in the natural gas cabin of urban underground utility tunnels based on CFD simulations, Tunn. Undergr. Space Technol. 109 (2021) 103748.
[34] X. Fan, J. Yang, H. Zhang, Z. Wan, J. Liu, Z. Liu, C. Zhu, W. Zheng, Prediction of back-layering length in subway tunnel with on-fire train running, Tunn. Undergr. Space Technol. 141 (2023) 105375.
[35] W. Liu, M. Liu, R. Chang, B. Yang, H. Cui, C. Li, H. Zhang, Study on moving fire smoke characteristics and mechanical ventilation system of tunnel, Fire Saf. J. 141 (2023) 103932.
[36] B. Magnussen, B. Hjertager, On mathematical modeling of turbulent combustion with special emphasis on soot formation and combustion, Symp. Int. Combust. 16 (1977) 719–729.
[37] T. Xu, D. Zhao, H. Tao, P. Lei, Extended CFD models for numerical simulation of tunnel fire under natural ventilation: comparative analysis and experimental verification, Case Stud. Therm. Eng. 31 (2022) 101815.
[38] R.E. Bensow, C. Fureby, M. Liefvendahl, T. Persson, A Comparative Study of RANS, DES and LES, (n.d.)..
[39] E. Lynch, M. Smith, Hybrid RANS-LES turbulence models on unstructured grids, in: 38th Fluid Dyn. Conf. Exhib., American Institute of Aeronautics and Astronautics, Seattle, Washington, 2008.
[40] J. He, X. Huang, X. Ning, T. Zhou, J. Wang, R.K.K. Yuen, Modelling fire smoke dynamics in a stairwell of high-rise building: effect of ambient pressure, Case Stud. Therm. Eng. 32 (2022) 101907.
[41] D. Moreno-Boza, W. Coenen, J. Carpio, A.L. Sánchez, F.A. Williams, On the critical conditions for pool-fire puffing, Combust. Flame 192 (2018) 426–438.
[42] C. Caliendo, G. Genovese, I. Russo, A 3D CFD modeling for assessing the effects of both longitudinal slope and traffic volume on user safety within a naturally ventilated road tunnel in the event of a fire accident, IATSS Res. 46 (2022) 547–558.
[43] S.K. Khattri, From small-scale tunnel fire simulations to predicting fire dynamics in realistic tunnels, Tunn. Undergr. Space Technol. 61 (2017) 198–204.
[44] L. Yu, Y. Chen, S. Chen, Y. Zhang, H. Zhang, C. Liu, Numerical analysis of the performance of a PID-controlled air curtain for fire-induced smoke confinement in a tunnel configuration, Fire Saf. J. 141 (2023) 103930.
[45] A. Król, W. Jahn, G. Krajewski, M. Król, W. Węgrzyński, A study on the reliability of modeling of thermocouple response and sprinkler activation during compartment fires, Buildings 12 (2022) 77.
[46] J. Quintiere, Fundamentals of Fire Phenomena, first ed., Wiley, 2006.
[47] W. Zhao, R. Zong, X. Fan, X. Zhao, Y. Deng, X. Zhang, Scaling applications of wall parameters in a tunnel fire, Tunn. Undergr. Space Technol. 106 (2020) 103585.
[48] S. Welch, P. Rubini, Three-dimensional simulation of a fire-resistance furnace, Fire Saf. Sci. 5 (1997) 1009–1020.
[49] K. McGrattan, G. Forney, Fire Dynamics Simulator (Version 4): User's Guide, National Institute of Standards and Technology, Gaithersburg, MD, 2004.